Frame deformations control based on reduced order Thermo-elastic models

W.W.J. Aarden[1], T. Ruijl[1]

[1]MI-partners, The Netherlands

w.aarden@mi-partners.nl

INTRODUCTION

Thermal induced deformations in high precision systems can be one of the dominant contributions to the overall positioning accuracy. To reduce these errors, real-time error compensation methods [1] or even active control can potentially be used. Both (1) compensation and (2) correction is used and explained in this paper. This article will focus on using temperature sensors, in combination with a reduced order thermo-elastic model, to estimate displacements and tilts of an optical unit and use this information to correct or compensate in-plane displacement errors at the stage. The compensation (1) is done by adjusting the setpoint position of the high precision stage. The thermal correction (2) is based on temperature control of water cooled plates in combination with local fluid stream heaters at several frame positions.

CASE

To investigate the potential of the compensation and correction methods, a realistic high precision system operating in a high vacuum environment is taken into consideration.

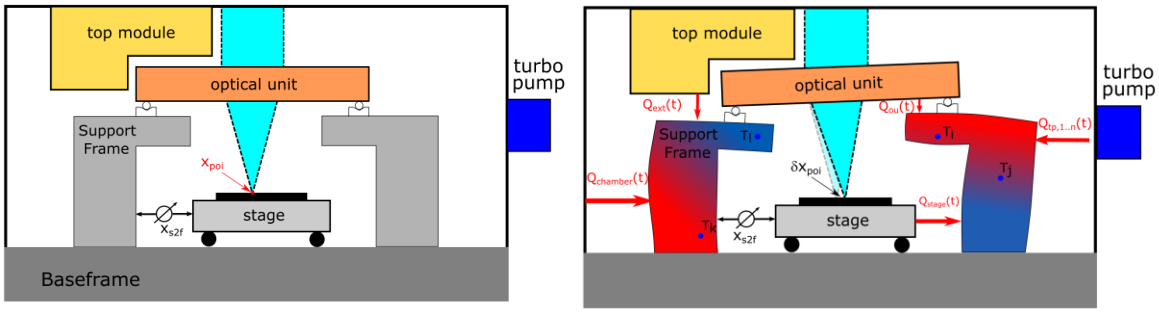

Figure 1: Left: Schematic depiction of the precision system. Right: Thermal induced frame deformations, resulting in relative errors at the POI, δx_{poi}.

The system consists of a high precision stage, actively positioned underneath an optical unit in multiple degrees of freedom, while using a stage position metrology system. This metrology system measures the stage position with respect to the support frame, x_{s2f}. The systems performance is defined as the positioning error between the point of interest (POI), x_{POI}, located on the top surface of the stage and the focus point of the optical unit, see left figure 1.

In addition there is an optical unit that is kinematically supported on the heavy and stiff support frame. The environment surrounding the frame consists of several surfaces that have a varying temperature. By thermal radiation they will generate multiple time varying heat loads, $Q_i(t)$, onto the support frame . In combination with the thermal boundary conditions, i.e. frame connection to the base frame, there will be temperature gradients in the frame structure. These gradients induce frame deformations, resulting in displacements and tilts of the optical unit, and finally leading to errors at the POI, δx_{poi}. See right figure 1. Due to the arrangement of the stage metrology system, such δx_{poi} cannot be observed and therefore cannot be compensated.

The first goal is to estimate the mechanical POI displacements induced by the temperature field inf the frame, while using a limited number of temperature measurements. Where the second goal focusses on a control strategy to minimize this displacement by means of the thermal actuators.

The rest of the article is organized as follows. First the thermo-elastic 3D CAD and FE model is described. Secondly the model order reduction technique is described, followed by the used sensor placement strategy. Next the results of the several numerical experiments are presented including the controller design and its performance. Concluding with final thoughts and future work.

THERMO-ELASTIC MODEL

Based on the presented precision system a high fidelity 3D finite element model (FEM) of the support frame is created and can be seen in figure 2. The support frame consists of three aluminium solid pillars ($h = 350\,mm$) that are connected to a base frame. The three support pillars are interconnected by three aluminium beams to supply additional structural stiffness. The three kinematic mounts lie on a radius of 150 mm.

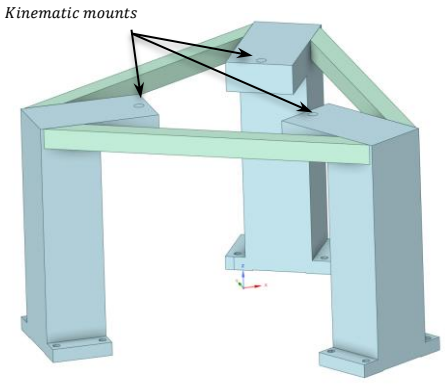

Figure 2: 3D CAD model of the support frame.

The pillars and beams are made out of aluminium 6061-T6. The boundary conditions to the baseframe are modelled as a thermal convection with the baseframe reference temperature as input. The value of the heat transfer coefficient is derived from contact resistances given by bolted metal-metal

interfaces in vacuum. The thermal loads are estimated from a thermal simulation including radiation between the different environment surfaces, i.e. vacuum chamber, hot turbo pumps and top module. Figure 3 shows an overview of these heat loads and which surfaces they effect on the support frame. Additionally, there is a heat load that comes from the optical unit and enters through the kinematic mounts directly and has an average value of $Q_{ou} = 1.2\,W$. The total average heat load that enters the frame is $\hat{Q}_{total} = 4.98\,W$.

A structural-thermal coupled finite element model is created using ANSYS. This model, containing n_{nodes} nodes, can be used to calculate the deformations of the frame given the thermal boundary conditions and heat loads. The coupled thermo-elastic system in discrete form is given by

$$\begin{bmatrix} 0 & 0 \\ 0 & C_T \end{bmatrix} \begin{bmatrix} \dot{u} \\ \dot{T} \end{bmatrix} = \begin{bmatrix} -K_{uu} & K_{uT} \\ 0 & -K_{TT} \end{bmatrix} \begin{bmatrix} u \\ T \end{bmatrix} + \begin{bmatrix} 0 \\ B_T \end{bmatrix} w \qquad (1)$$

Where u represents the vector of the nodal displacement field in the X,Y and Z directions and T is vector of the nodal temperature field. The matrices C_T, K_{TT} and B_T denote the thermal capacitance, conductance and input matrix. The matrices K_{uu} and K_{uT} are the structural stiffness matrix and the thermo-elastic coupling matrix respectively. The inputs are given by w, which consist of the reference temperature of the boundary conditions and the defined heat loads. By defining the combined state vector $x = [u, T]^T$, the system can be written as

$$E\dot{x} = Ax + Bw \qquad (2)$$

Where $E,\ A \in \mathbb{R}^{n\times n}$ and $B \in \mathbb{R}^{n\times m}$, with $n = 4n_{nodes}$ and m the number of inputs.

The in-plane POI displacements, u_{POI} that define the systems performance can be found by using an additional output equation

$$u_{POI} = Hx \qquad (3)$$

Where $H \in \mathbb{R}^{p\times n}$ maps the state vector x to the in-plane POI displacements, i.e. $p = 2$. So given a temperature field $\hat{T}$ the POI displacement can be expressed as

$$u_{POI} = H_{poi} G_{uT} \hat{T} \qquad (4)$$

With $G_{uT} = K_{uu}^{-1} K_{uT}$ the mapping from temperature to displacements and H_{poi} is the observation matrix.

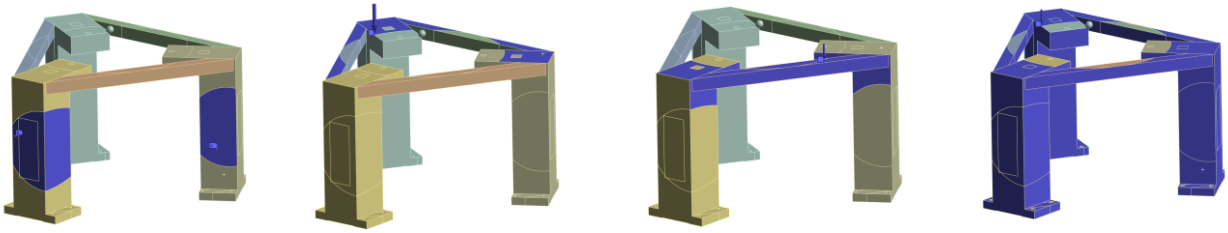

(a) (b) (c) (d)

Figure 3: Overview of the heat loads, (a) 2x turbo pumps $Q_{tp} = 1.3W$, (b) Top module top $Q_{tm} = 0.9\,W$, (c) Top module side $Q_{tp_{side}}(t) = 0.75 \pm 0.65\,W$, (d) Vacuum chamber $Q_{vc}(t) = 0.83\ W$

MODEL ORDER REDUCTION

In order to have an accurate thermo-elastic model that can be used to analyse the performance of the system for different sets of load cases, to be efficiently used in a sensor placement algorithm and to be able to design robust controllers, a reduced order model (ROM) is required that can capture the coupled thermo-elastic physics accurately within a certain frequency range, see for more information and an overview [3,4]. Model order reduction is aimed to reduce the dimension of dynamical systems of the form given by (2) and (3).

The reduction methods aim to find projection matrices, $V, W \in \mathbb{R}^{n\times k}$ with $k \ll n$ such that the ROM is given by

$$\hat{E}\dot{z} = \hat{A}z + \hat{B}w, \quad \hat{y} = \hat{H}z \tag{5}$$

where

$$\hat{E} = W^T EV \in \mathbb{R}^{k\times k} \quad \hat{B} = W^T B \in \mathbb{R}^{k\times m}$$
$$\hat{A} = W^T A \in \mathbb{R}^{k\times k} \quad \hat{H} = HV \in \mathbb{R}^{p\times k}$$

with the requirement $|\hat{y} - y| < \varepsilon$. Depending on the intended use of the ROM, this requirement is to be interpreted differently. Several methods are available to create ROMs, e.g. balanced truncation, modal superposition method, proper orthogonal decomposition and moment matching. Both, the modal superposition as the moment matching methods, were investigated for the sensor placement and the controller design. It was found that the most computational efficient and accurate method is the moment matching (MM). The key idea of the MM method is to match the so-called moment of the system's transfer function. Given the input-output transfer function of the system

$$P(s) = (sC_T + K_{TT})^{-1}B_T \tag{6}$$

of the thermal system, this can be written as a Neumann series

$$P(s) = \sum_{j=0}^{\infty} m_j (s - s_0)^j \tag{7}$$

where the moments m_j are given by

$$m_j = (-(s_0 C_T + K_{TT})^{-1} C_T)^j (s_0 C_T + K_{TT})^{-1} B_T. \tag{8}$$

The reduction method aims to find a ROM (6) such that a number of moments, $\hat{m}_j$

$$\hat{m}_j = \left(-\left(s_0\hat{C} + \hat{K}\right)^{-1}\hat{C}\right)^j \left(s_0\hat{C} + \hat{K}\right)^{-1}\hat{B}_T \tag{9}$$

of the ROM transfer function $\hat{P}(s) = \left(s\hat{C} + \hat{K}\right)^{-1}\hat{B}$ matches the moments m_j of the original transfer function $G(s)$. The computation of the projection matrix V for large models can efficiently be computed by using Krylov subspace based methods. Calculating a projection matrix V in this way

$$span(V) = \mathcal{K}[(-(s_o C_T + K_{TT})^{-1} C_T), (-(s_o C_T + K_{TT})^{-1} B_T)] \quad (10)$$

ensures that the first k moments are matched. The expansion point s_0 can be arbitrary, but given the fact that thermal systems have slow transient behaviour, $s_0 = 0$ is most commonly used.

With an ANSYS to Matlab internal developed toolbox the single sided Krylov basis temperature shapes can be efficiently and accurately computed. Figure 4 shows the first 4 temperature shapes of the support frame. For the rest of the article the so-called single-sided projection, i.e. $W = V$, is used. Using only V as the projection matrix, ensures that the ROM is stable, given an underlying stable full order model (FOM), see [4].

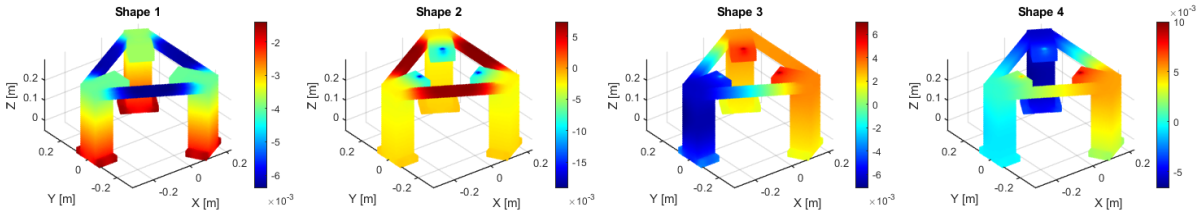

Figure 4: the first 4 Krylov temperature shapes

SENSOR PLACEMENT STRATEGY

The sensor placement strategy is based on the work presented in [2,7]. The main steps are summarized in the next section. To make the sensor placement problem computational attractable it is essential to use ROMs with their projection matrix V. A detailed discussion on this can be found in [7]. Using the ROM, the POI in-plane displacement estimation now becomes

$$u_{POI} \approx H_{poi} G_{uT} V \tilde{T} \quad (11)$$

If the reduced temperature field at each timestep $\tilde{T}(t)$ can be estimated accurately, then instantaneously the $u_{POI}(t)$ is known at the timestep. The estimation of $\tilde{T}$ is achieved by solving the least-squares problem

$$\min_{\tilde{T} \in \mathbb{R}^k} \frac{1}{2} \sum_{i=1}^{n_s} \left(V(x_i)\tilde{T} - T_{m,i} \right)^2 \quad (12)$$

here $T_{m,i}$ is the ith temperature measurement at location x_i on a allowed surface S, with $i = 1 \dots n_s$ and $V(x_i) = V(i,:)$, i.e. the row selected by

the ith sensor location. Note that the nodes of the finite element mesh determined by S restrict the possible locations for x_i. Let $X = [x_1, \dots, x_{n_s}]$ be the selected positions, from the solution of (13) the estimator for the reduced temperature field $\tilde{T}$, $E_{\tilde{T}}(X)$ can be constructed and is given by

$$E_T(X) = [\vartheta(X)^T\vartheta(X)]^{-1}\vartheta(X)^T T_m \qquad (13)$$

here $\vartheta(X)$ is the Jacobian of the residuals with respect to the unknows, components of $\tilde{T}$, i.e.

$$\vartheta(X) = [V(X,1) \dots V(X,k)] \in \mathbb{R}^{n_s \times k} \qquad (14)$$

and $V(X,j) = \begin{bmatrix} V(x_1,j) & \dots & V(x_{n_s},j) \end{bmatrix}^T$ and T_m is the vector of the measurements. The estimator of the POI displacements, $E_{u_{POI}}(X)$, can be defined using (12)

$$E_{u_{POI}}(X) = H_{poi}G_{uT}V[\vartheta(X)^T\vartheta(X)]^{-1}\vartheta(X)^T T_m \qquad (15)$$

Given the estimator of u_{POI} the precision of the estimation can be assessed from its covariance matrix [2], i.e.

$$Cov_u(X) = \mu_T^2 H_{poi}G_{uT}V[\vartheta(X)^T\vartheta(X)]^{-1}\left(H_{poi}G_{uT}V\right)^T \qquad (16)$$

Considering that the temperature measurement errors are independent and distributed random variables with a normal distribution of zero mean and variance μ_T^2. Here the choice of V and the selected positions X determines $Cov_u(X)$.

The sensor placement algorithm has a sequential placement approach, i.e. given a set of $i-1$ already selected sensor positions $[x_1, \dots, x_{i-1}]$, find a new location x_i that minimizes the following subproblem

$$\min_{x_i \in S} f\left(Cov_u(x_1, \dots, x_{i-1}; x_i)\right) \qquad (17)$$

here the optimality criteria f is defined as $f_D(Cov) = \log(det(Cov))$. For more detailed information regarding the algorithm see [7].

RESULTS

First step is to determine the reduced order size k. For this problem the frequency content of the heat loads are considered. It is known from additional analysis that there is frequency content for $f_w < 4\ mHz$. In combination with the following norm on the relative transfer function error

$$\frac{\left\|P(j2\pi f_w) - \hat{P}(j2\pi f_w)\right\|_\infty}{\|P(j2\pi f_w)\|_\infty} < \varepsilon \qquad (18)$$

the order k can be found given a certain ε. Using a $\varepsilon < 10^{-3}$ the minimum order is found to be $k = 65$. Next step is to use the sensor placement strategy to find the minimum set of required sensors. This is done in combination with additional constraints in order to make it a viable solution for the system. 1) The variance $Var(u_{POI}) < (3\sigma_u)^2$, with $3\sigma_u = 0.05\ \mu m$ and $3\sigma_T < 1mK$, such that the target performance can be achieved, 2) the system has to operate for a long period of time, thus the

impact of temperature drift from the sensors is required to be minimal and has the same requirement as the variance, i.e. $3\sigma_{drift} < 0.1\ \mu m$, with worst case sensor drift of $\pm\ 10\ mK$ and 3) with $n_{sensors}$ the temperature estimator (14) can estimate the reduced $\tilde{T}$ for a static heat load with $\left\|\tilde{T} - E_T(X)\right\|_2 < 10\ \mu K$. The minimum required number of sensors was found to be $n_s = 12$ and figure 5 shows the optimal sensor locations on the outer surface of the support frame.

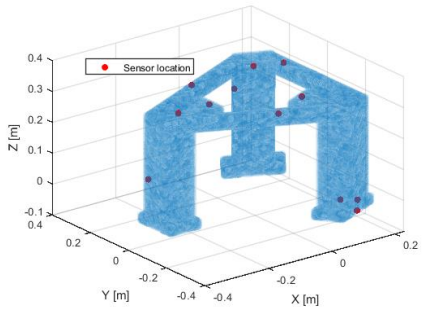

Figure 5 Optimal sensor locations, $\mathrm{n_s} = 12$

The evolution of the sensor placement is shown in figure 6. Here it can be seen that the target for $Var(u_{POI})$ with $3\mu_T = 1\ mK$ can be achieved for a certain selection of sensors, however for $n_s = 16 \ldots 18$, the noise level of the y_{POI} estimation becomes too large. The static error temperature norm shows that a minimum number of sensors $n_s \geq 12$ is required in order to estimate the reduced temperature field $\tilde{T}$ sufficiently accurate. To guarantee sensor drift target the correct number of sensors should be $10 < n_s < 15$.

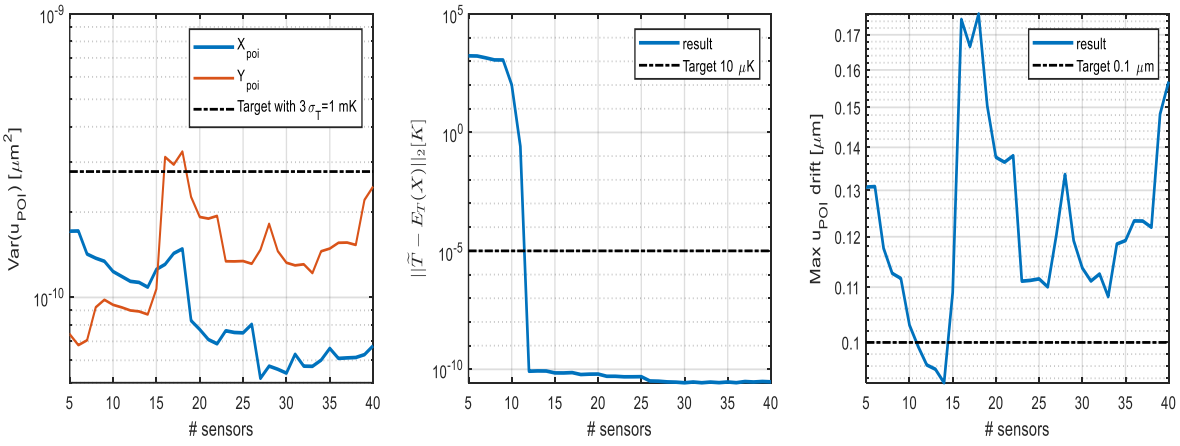

Figure 6: Plots of the variance $\mathrm{Var(u_{POI})}$, static temperature error $\left\|\mathrm{\tilde{T} - E_T(X)}\right\|_2$ and the maximum POI drift for $\mathrm{\Delta T = \pm 10\ mK}$ sensor drift.

The final performance using $n_s = 12$ for multiple different loadcases has been simulated and a worst-case result for u_{POI} is shown in figure 7. Both the X and Y estimation error is below the $0.05\ \mu m$ target.

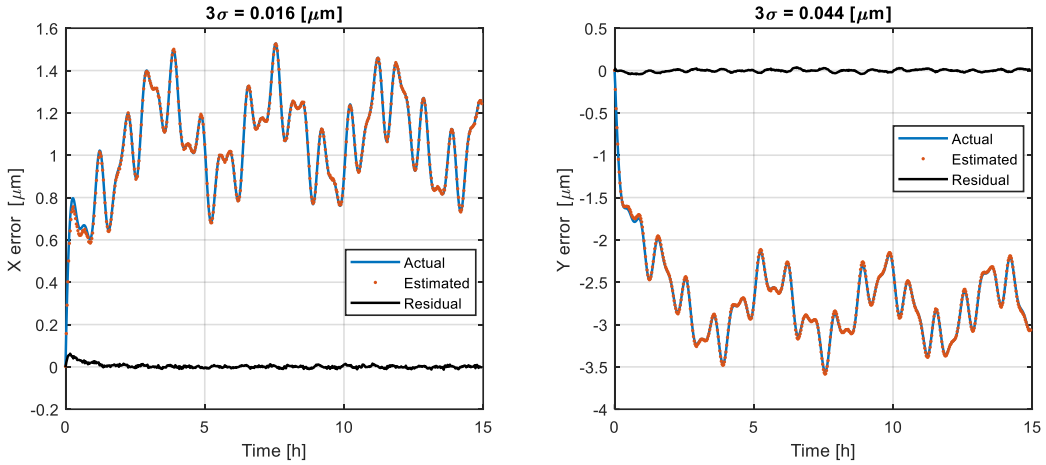

Figure 7. u_{POI} estimation performance for $n_s = 12$ and $3\mu_T = 1$ mK.

THERMAL CONTROL

The estimated u_{POI} can be used to update the stage setpoint in order to compensate for the thermal induced deformations. Alternatively a multiple input, multiple output controller can be implemented that uses the u_{POI} estimated values and actively attenuates disturbances to reduce the u_{POI} displacements and minimizes the average frame temperature increase. In order to minimize the radiation load toward other sensitive equipment. For this purpose, three water cooled plates are added to the support pillars (see rectangular face in figure 4), with a fixed water temperature that is lower than the reference temperature of $22°C$. The water temperature can be locally heated using local fluid heaters. This setup allows the pillars to actively cool and heat up as required from the controller. The added thermal dynamics of the fluid heater is added to the overall system dynamics.

Using an actuator decoupling strategy 2 decentralized controllers can be designed with a controller bandwidth of 1mHz. The maximum achievable bandwidth is limited due to the relatively large distance of the cooling plates with respect to the kinematic mounts, together with the discrete time controller delay. Figure 8 shows the closed loop performance compared to the no control performance. The limitation on the achievable bandwidth results in a residual error of $< 0.2\ \mu m$.

CONCLUSION & FUTURE WORK

The use of temperature sensors in combination with a thermo-elastic model shows promising performance. With state-of-the-art available temperature sensors including realistic measurement noise and drift, the estimation performance of $3\sigma_u \leq 0.05\ \mu m$ can be achieved by using a minimum set of $n_s = 12$.

Controller implementation using the estimation of u_{POI} is also possible, however the final performance ($3\sigma_u \leq 0.2\ \mu m$) is mainly limited due to the cooling plate locations. Achieving better

performance is a topic for future work. Here a focus will be on actuator placement strategies, in order increase the effectiveness of a set of cooling plates. Parallel to this work, the use of thermal-elastic system identification will be investigated. Where the focus will be on model validation and calibration, thus making the deformation estimation viable for real applications.

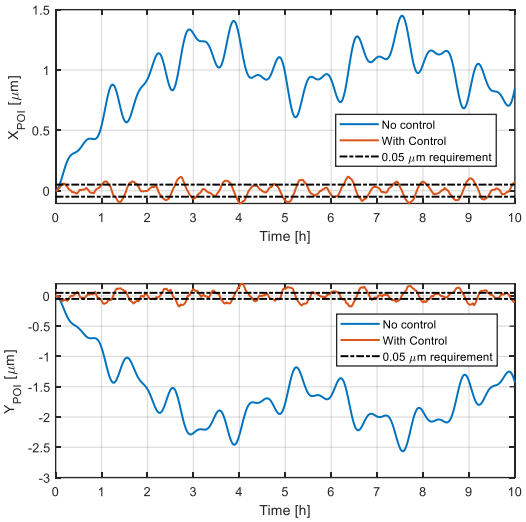

Figure 8: Closed loop performance.

REFERENCES

[1] Koevoets, A. H., Eggink, H. J., Van der Sanden, J., Dekkers, J., & Ruijl, T. A. M. Optimal sensor configuring techniques for the compensation of thermo-elastic deformations in high-precision systems. 13th International Workshop on Thermal Investigation of ICs and Systems (THERMINIC); 2007: 208-213.

[2] Benner, P., Herzog, R., Lang, N., Riedel, I., Saak, J. Comparison of model order reduction methods for optimal sensor placement for thermo-elastic models. Engineering Optimization; 2019: 51(3), 465-483.

[3] IEEE.Antoulas, A. C. Approximation of large-scale dynamical systems. Society for Industrial and Applied Mathematics; 2005.

[4] Antoulas, A. C., Sorensen, D. C., Gugercin, S. A survey of model reduction methods for large scale systems. Contemporary mathematics 2001; 280: 193-220.

[5] Aarden W., Bukkems B., Limpens M. and Ruijl T. Applied thermo-elastic model reduction Euspen Thermal Issues Proceedings 2020; 71-74

[6] Van der Sanden J, Philips P. FEM model based POD reduction to obtain optimal sensor locations for thermo-elastic error compensation. Proceedings of the 13th euspen International Conference; 2013

[7] Herzog, R. and Riedel I., Sequentially Optimal Sensor Placement in Thermoelastic Models for Real Time Applications. Optimization and Engineering 16 (4): 737-766